

# Magnetic Reconnection and Particle Acceleration in Active Galactic Nuclei

R. Schopper, H. Lesch, and G.T. Birk

Institut für Astronomie und Astrophysik der Universität München, Scheinerstraße 1, D-81679 München, Germany

Received date ; accepted date

**Abstract.** Magnetic field-aligned electric fields are characteristic features of magnetic reconnection processes operating in externally agitated magnetized plasmas. An especially interesting environment for such a process are the coronae of accretion disks in active galactic nuclei (AGN). There, Keplerian shear flows perturb the quite strong disk magnetic field leading to intense current sheets. It was previously shown that given field strengths of 200 G in a shear flow, reconnection driven magnetic field aligned electric fields can accelerate electrons up to Lorentz factors of about 2000 in those objects thus providing us with a possible solution of the injection (pre-acceleration) problem. However, whereas in the framework of magnetohydrodynamics the formation of the field-aligned electric fields can be described consistently, the question has to be addressed whether the charged particles can really be accelerated up to the maximum energy supplied by the field-aligned electric potentials, since the accelerated particles undergo energy losses either by synchrotron or inverse Compton mechanisms. We present relativistic particle simulations starting from electric and magnetic fields obtained from magnetohydrodynamic simulations of magnetic reconnection in an idealized AGN configuration including nonthermal radiative losses. The numerical results prove that the relativistic electrons can be effectively accelerated even in the presence of an intense radiation bath. Energies from 50MeV up to 40GeV can be reached easily, depending on the energy density of the photon bath. The strong acceleration of the electrons mainly along the magnetic field lines leads to a very anisotropic velocity distribution in phase space. Not even an extremely high photon energy density is able to completely smooth the anisotropic pitch angle distribution which is characteristic for quasi monoenergetic particle beams.

**Key words:** AGN – Particle Acceleration – Magnetic Reconnection – Particle Simulations

## 1. Introduction

Active galactic nuclei (AGN) can be regarded as accreting supermassive black holes surrounded by accretion disks (Camenzind 1990; Miyoshi et al. 1995; Burke and Graham-Smith 1997 and references therein). Relativistic electrons in AGN reveal themselves by hard X-ray (probably due to pair production (cf. Svensson 1987; Done and Fabian 1989)) and  $\gamma$ -ray emissions as well as radio observations of superluminal motions (e.g. Abraham et al. 1994). The  $\gamma$ -radiation observed from quasars and blazars may originate in a distance  $R$  of  $10^{2-3}$  gravitational radii from the central engine (Dermer and Schlickeiser 1993). At that distance no significant pair production happens but relativistic leptons scatter via the inverse Compton process the IR-UV radiation of the accretion disk within a relativistically moving jet. It is well known that “standard” mechanisms for the acceleration of high energy leptons, as diffusive shock wave acceleration and resonant acceleration by magnetohydrodynamical (MHD) turbulence can only work efficiently for Lorentz factors larger than  $\gamma_{\text{crit}} \simeq m_p/m_e$  (where  $m_p$  and  $m_e$  denote the proton and electron masses). Consequently, charged particles accelerated via shocks or MHD turbulence have to be pre-accelerated which confronts us with the **injection problem** (Blandford 1994; Melrose 1994) in the AGN context.

In a differentially rotating magnetized accretion disk gas, the evolution of a magnetized corona is quite hard to suppress (Galeev et al. 1979; Stella & Rosner 1984). Driven by the buoyancy force magnetic flux tubes ascend into the disk corona, thereby their footpoints are sheared by the differential rotation of the disk. Either by internal shear or by encountering already present magnetic flux, magnetic reconnection and accompanied rapid dissipation of magnetic energy happens in the coronal plasma. Such a behavior can be studied with great detail for example in the solar corona (Parker 1994 and references therein). In a recent contribution we investigated the possible role of magnetic field-aligned electric fields ( $E_{\parallel}$ ) in the context of magnetic reconnection operating in AGN coronae for the pre-acceleration of leptons (Lesch and Birk 1997; hereafter LB). It could be shown that field-aligned electric potential structures in relatively thin current sheets form. For reasonable physical parameters such electric potentials are strong enough to accelerate electrons up to  $\gamma \approx 2000$ , in principle. However,

in the framework of MHD the actual energies of the accelerated particles cannot be calculated. It is the aim of the present contribution to corroborate the model introduced in LB with the help of relativistic particle simulations by taking macroscopic electric and magnetic field configurations obtained by the MHD simulations as an input.

In the next section we resume the MHD model in a nutshell and present the details of the resulting three-dimensional electric and magnetic fields. In Sec. 3 we discuss our approach to the numerical study of high-energy particles and show the numerical results dwelling on particle spectra and energies. Eventually, we discuss our findings in Sec. 4.

## 2. The MHD model for magnetic reconnection in the corona of an accretion disk

The MHD framework for the particle simulations is modeled by means of a 3D resistive MHD code that integrates the one-fluid balance equations (e.g. Krall and Trivelpiece 1973):

$$\frac{\partial \rho}{\partial t} + \nabla \cdot (\rho \mathbf{v}) = 0 \quad (1)$$

$$\frac{\partial}{\partial t}(\rho \mathbf{v}) + \nabla \cdot (\rho \mathbf{v} \mathbf{v}) = -\nabla p + \frac{1}{c} \mathbf{j} \times \mathbf{B} \quad (2)$$

$$\frac{\partial p}{\partial t} + \nabla \cdot (p \mathbf{v}) = \frac{2}{3}(-p \nabla \cdot \mathbf{v} + \eta j^2) \quad (3)$$

$$\frac{\partial \mathbf{B}}{\partial t} = \nabla \times (\mathbf{v} \times \mathbf{B}) - \frac{c^2}{4\pi} \nabla \times (\eta \mathbf{j}) \quad (4)$$

where  $\rho$ ,  $\mathbf{v}$ ,  $p$ ,  $\mathbf{B}$ ,  $\mathbf{j}$  and  $\eta$  denote the plasma mass density, velocity and pressure, the magnetic field, the electric current density and the electrical resistivity.

The scenario we have in mind can be briefly described as follows (for details see LB): Different convective plasma motions at different regions of an AGN corona or differential shear motion of the disk result in a sheared magnetic field and consequently, in the formation of field-aligned electric current sheets. When this convective shear motion is strong enough to result in a supercritical current density (drift velocity larger than the local sound velocity  $c_s = \sqrt{k_B T_e / m_p}$  current-driven microinstabilities are excited which lead to anomalous electrical resistivity (e.g. Huba 1985; Benz 1993). The formation of localized regions of anomalous dissipation or, more general, the local violation of ideal Ohm's law, can be regarded as the necessary onset condition for magnetic reconnection (Schindler et al. 1988, 1991). During the dynamical evolution of the reconnection process very localized acceleration regions ( $\mathbf{E}_{\parallel} \neq 0$ ) form.

Since we want to concentrate on a single sheared coronal loop which is represented by a current-carrying magnetic flux tube we start from an appropriate idealized initial configuration for the MHD simulation run which is characterized by a homo-

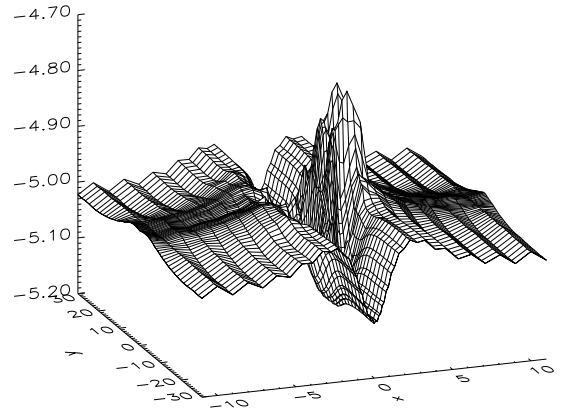
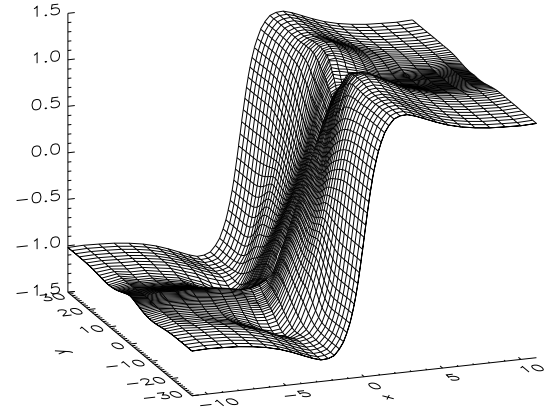
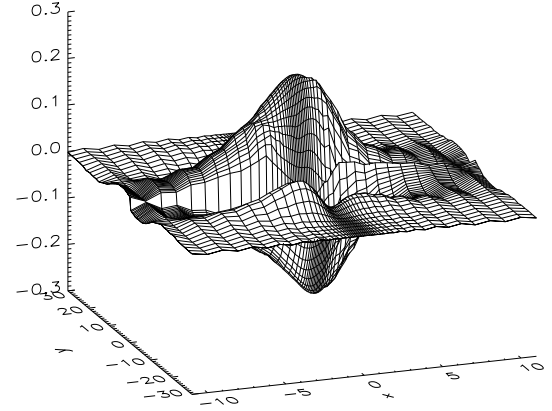


**Fig. 1.** The  $x$ -,  $y$ - and  $z$ -component (from top to bottom) of the reconnection magnetic field at the height of the central reconnection region after  $t = 120\tau_A$ .

geneous plasma and a force-free magnetic field (cf. Birk and Otto 1996; LB):

$$\mathbf{B} = B_{y0} \tanh(x) \mathbf{e}_y - \sqrt{B_{z0}^2 + \frac{B_{y0}^2}{\cosh^2(x)}} \mathbf{e}_z \quad (5)$$

where  $B_{z0} = 5$  and  $B_{y0} = 1$  denote the normalized constant main component and the shear (toroidal) component of

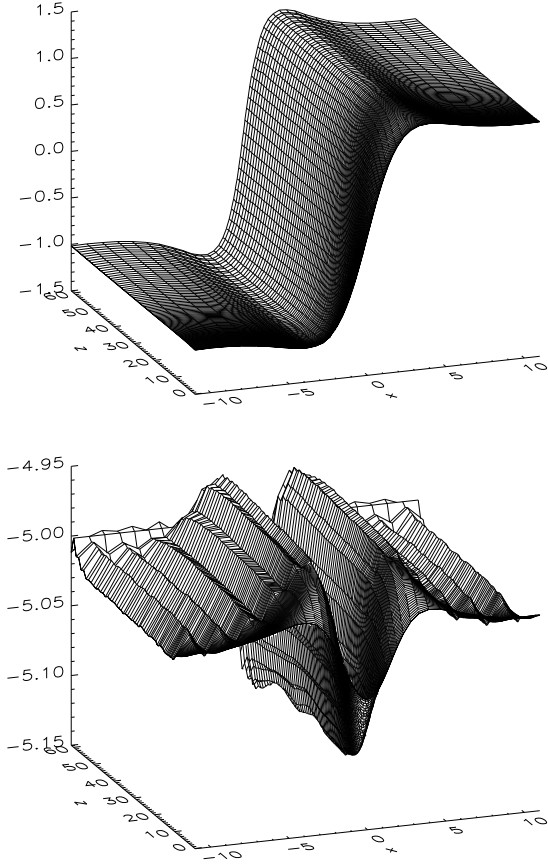


**Fig. 2.** The  $y$ - and  $z$ -component of the reconnection magnetic field at the  $y = 0$ -half plane (i.e. the middle on the of the central reconnection region) after  $t = 120\tau_A$ .

the magnetic field, respectively. As discussed in LB we choose for the half-width of the current sheet  $w \approx 10^7 \text{cm}$ , a shear magnetic field of  $B_{y0} = 200 \text{G}$ , a particle density of  $n = 3 \cdot 10^5 \text{cm}^{-3}$  and  $10^4 \text{statamp cm}^{-2}$  for the critical current density of  $j_{\text{crit}}$ , which corresponds to an electron temperature of  $6 \cdot 10^7 \text{K}$  (cf. Ulrich 1991; Nandra and Pounds 1994). The magnetic Reynolds number is chosen as  $S = 4\pi v_A w / \eta c^2 = 10^3$ .

The initial equilibrium configuration is perturbed by some sheared flow:

$$v_y(x, z, t) = v_{y0} \frac{\tanh(2x)}{\cosh^2\left(\frac{x}{3}\right)} e^{-\frac{z}{6}} \quad (6)$$

with an amplitude chosen as  $v_{y0} = 0.5\%$  of the shear Alfvén velocity  $v_A = B_{y0} / \sqrt{4\pi\rho}$ . This perturbation is transported down along the main component of the magnetic field via shear Alfvén waves during the dynamical evolution. An anomalous resistivity will be switched on when the current density exceeds the critical value  $j_{\text{crit}}$ . The resistivity is localized in height along the poloidal component of the magnetic field in order to model an acceleration region of the length of  $40w$  as well as in the  $y$ -direction (for technical details we again refer to LB). During the dynamics reconnection electric and magnetic fields

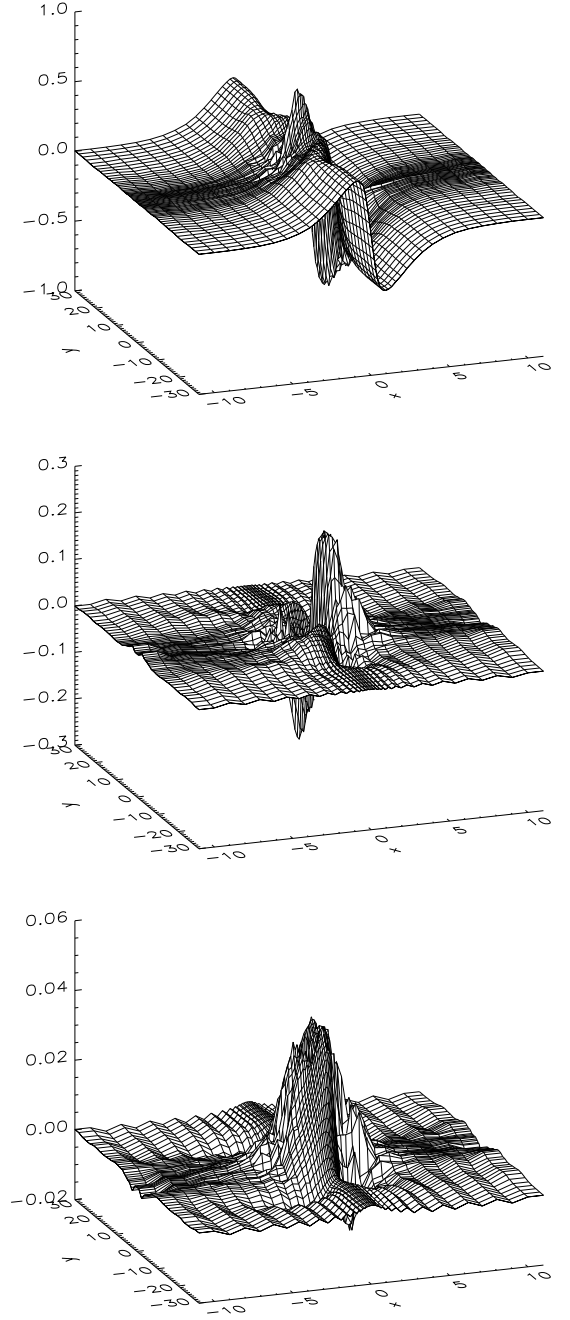


**Fig. 3.** The  $x$ -,  $y$ - and  $z$ -component (from top to bottom) of the reconnection electric field after  $t = 120\tau_A$ .

evolve which can be used as an input configuration for the particle simulation of the acceleration of high-energy electrons in the reconnection region. A snapshot after  $t = 120$  dynamic times (i.e.  $\tau_A = w/v_A$ ) of the Cartesian components of the magnetic and electric fields are shown in Figures 1–3. The resulting  $x$ -component of the magnetic field shows the typical bipolar reconnection characteristic (Fig. 1, top panel). The middle panel of Fig. 1 shows the  $y$ -component of the magnetic field associated with the current sheet and the lower panel shows the

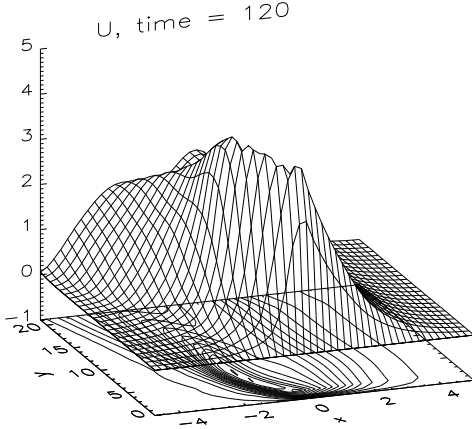


**Fig. 4.** The generalized electric potential  $U$  after  $t = 120\tau_A$ .

$z$ -(poloidal) component. Fig. 2 shows the  $y$ - and  $z$ -component of the magnetic field at the  $y = 0$ -half plane. The  $y$ -component is enhanced locally due to the sheared flow applied at the upper boundary and transported along the poloidal component of the magnetic field via shear Alfvén waves. The three-dimensional electric vector field at the height of the central reconnection region is illustrated in Fig. 3. The convective  $x$ -component (top panel) is the result of the applied sheared flow and the divergent reconnection flow whereas the convective  $y$ -component (middle panel) is due to the convergent ( $v_x(x)$ ) reconnection flow. The dominant accelerating component is  $E_z$  (lower panel) which is caused by the finite anomalous electrical resistivity  $E_z \sim \eta j_z$  and accordingly localized in the  $x$ - and  $y$ -direction.

The generalized field-aligned electric potential in normalized units  $U = -\int E_{\parallel} ds$  ( $ds$  is a magnetic field line element) associated with the electric and magnetic fields is illustrated in Fig. 4. It is this elongated relatively thin potential structure by which the electrons are accelerated as will be discussed in the next section.

### 3. Particle simulations

For the sake of simplicity, we perform our simulations as relativistic test particle simulations. This means, that any interaction between the simulated particles are neglected, as well as the backreaction of the considered particles on the electromagnetic fields. In our calculations we use the stationary fields, which are explained in Sec. 2, simply as the "stage" for the accelerated charged particles.

In addition to the acceleration force, we consider the radiative losses in our simulations, especially the synchrotron (SY) and the inverse Compton (IC)-losses. In particular, we are interested in the question:

Is magnetic reconnection able to accelerate particles to relativistic energies in the presence of synchrotron and inverse Compton losses?

#### 3.1. Momentum Equation and Numerical Procedure

From the mathematical point of view the problem of test particle simulation is an integration of the equations of motion for a single charged particle. Since we are dealing with test particles, we have to integrate:

$$\frac{d\mathbf{r}}{dt} = \mathbf{v} \quad (7)$$

$$\frac{d\mathbf{p}}{dt} = \mathbf{F}(\mathbf{r}, \mathbf{v}, t). \quad (8)$$

This simplifies our problem enormously. As usual, the vectors  $\mathbf{r}$ ,  $\mathbf{v}$  and  $\mathbf{p}$  represent position, velocity and momentum of the particle and  $\mathbf{F}$  is the force acting on the particle. We use the relativistic relations

$$\mathbf{p} = \frac{m_0 \mathbf{v}}{\sqrt{1 - \left(\frac{v}{c}\right)^2}} \iff \mathbf{v} = \frac{\mathbf{p}}{m_0 \sqrt{1 + \left(\frac{p}{m_0 c}\right)^2}} \quad (9)$$

between velocity and momentum, with the rest mass of the particle  $m_0$  and the velocity of light  $c$ .

The resulting force acting on the particle is, in the simplest case, given by the Lorentz force  $\mathbf{F}_L = q[\mathbf{E} + \mathbf{v}/c \times \mathbf{B}]$ , where  $q$  denotes the electric charge of the particle. This is used in calculations in which radiative loss processes are neglected. If we take these losses into account, we require in addition a radiative loss force, which describes the corresponding interaction between radiation field (photons) and particles. Such a force

$$\begin{aligned} \mathbf{F} = & \frac{2q^3 \gamma}{3mc^3} \left\{ \left( \frac{\partial}{\partial t} + (\mathbf{v} \cdot \nabla) \right) \mathbf{E} + \frac{1}{c} \mathbf{v} \times \left( \frac{\partial}{\partial t} + (\mathbf{v} \cdot \nabla) \right) \mathbf{B} \right\} \\ & + \frac{2q^4}{3m^2 c^4} \left\{ \mathbf{E} \times \mathbf{B} + \frac{1}{c} \mathbf{B} \times (\mathbf{B} \times \mathbf{v}) + \frac{1}{c} \mathbf{E} (\mathbf{v} \cdot \mathbf{E}) \right\} \\ & - \frac{2q^4 \gamma^2}{3m^2 c^5} \mathbf{v} \left\{ \left( \mathbf{E} + \frac{1}{c} \mathbf{v} \times \mathbf{B} \right)^2 - \frac{1}{c^2} (\mathbf{E} \cdot \mathbf{v})^2 \right\} \quad (10) \end{aligned}$$

can be found in Landau and Lifshitz (1951). It consists of *every* radiative loss process due to field-particle interaction, including SY- and IC-losses. Losses due to particle-plasma-wave interaction are not considered up to now.

The force given in Landau and Lifshitz (1951) is used here in a modified form. All terms with temporal or spatial derivatives are neglected, because the external fields are varying on great scales and it is very expensive to calculate those terms for the microscopic photon bath. So we consider the IC-losses by including an additional term, which describes the space- and time-averaged influence of the IC-losses of an isotropic photon bath with the energy density  $U_{\text{Rad}}$ . After some calculations this leads to the modified expression

$$\begin{aligned} \mathbf{F}_{\text{Rad}} \approx & \frac{2}{3} \frac{q^4}{m_0^2 c^4} \left\{ \mathbf{F}_L \times \mathbf{B} + \mathbf{E} \cdot (\mathbf{E} \cdot \boldsymbol{\beta}) \right. \\ & \left. - \gamma^2 \boldsymbol{\beta} \left[ F_L^2 + \frac{16}{3} \pi \beta^2 U_{\text{Rad}} - (\boldsymbol{\beta} \cdot \mathbf{E})^2 \right] \right\}. \quad (11) \end{aligned}$$

In this equation  $\beta = v/c$  is the velocity normalized to the speed of light.

The choice of numerical routines needs some comments. The routine, which is executed most, is the evaluation of the force  $\mathbf{F} = \mathbf{F}_L + \mathbf{F}_{\text{Rad}}$  at every timestep. This evaluation consists of an interpolation of the fields, which are known only on a grid. For the sake of rapidness we use a linear interpolation. This means, that at the grid boundaries the derivatives of our field quantities are not defined. For this reason we use a Runge–Kutta procedure of second order accuracy in combination with an adaptive stepsize control.

### 3.2. Particle simulations: Energies and Spectra

In our calculations we have obtained the following results. The SY–losses are completely unimportant in our AGN context. In Fig. 5 one can see clearly, that the curves without any

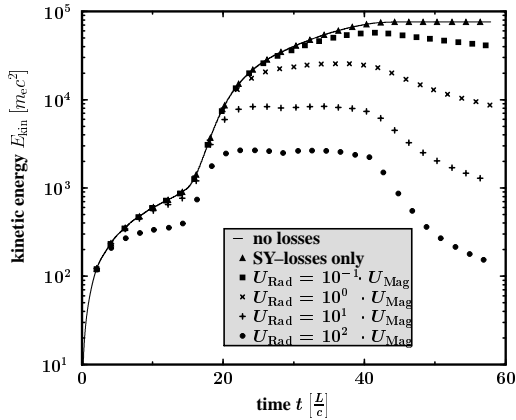


**Fig. 5.** Temporal evolution of the kinetic energy of a specific electron with respect to different loss processes and strengths

losses and with SY–losses only are nearly identical. In the following all energies are given in units of the rest energy of the electrons  $m_e c^2$  and  $U_{\text{Mag}}$  denotes the energy density of the magnetic field. For IC–losses the situation is completely different. The final energies decrease steadily with increasing photon energy density. However, even at the extreme value of  $U_{\text{Rad}} \approx 100 \cdot U_{\text{Mag}}$  the electrons gain some several tens of MeV. Anyway, one can clearly see that for reasonable photon energy densities ( $U_{\text{Mag}} \approx U_{\text{Rad}}$ ) a significant part of the injected electrons are accelerated towards GeV–energies. This can solve the injection problem.

The final energy spectra of the accelerated electrons for different strengths of IC–losses are shown in Fig. 6. For all spectra, the electrons were injected homogeneously distributed in the acceleration region with a velocity–distribution that corresponds to a Maxwell–distribution of temperature  $6 \cdot 10^8 \text{K}$ . In any case, the resulting final spectrum is a very broad one, which goes over some decades. The effects of IC–losses are clearly visible. The corresponding maximum of the distribu-

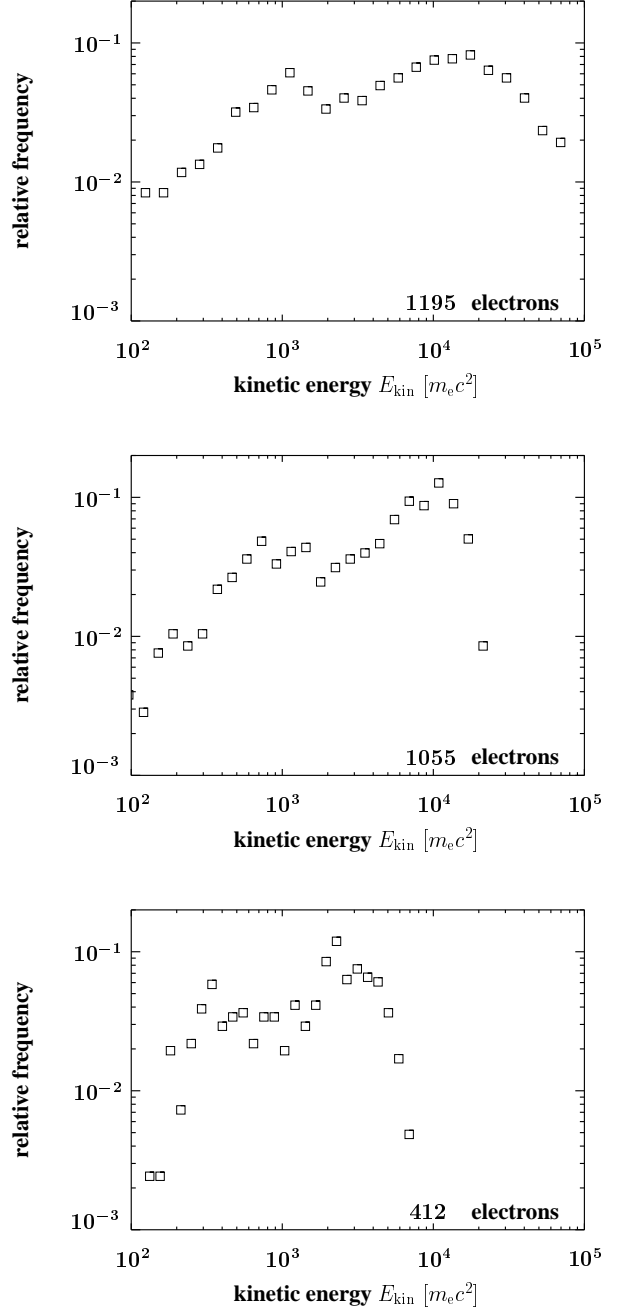


**Fig. 6.** Final energy distributions of the accelerated electrons for three different IC–loss strengths (top: no losses, middle:  $U_{\text{Rad}} = 10 \cdot U_{\text{Mag}}$ , bottom:  $U_{\text{Rad}} = 100 \cdot U_{\text{Mag}}$ )

tions is shifted towards lower energies with increasing photon densities. It shifts from about 8 GeV without energy losses to approximately 1 GeV at an energy density of  $100 U_{\text{Mag}}$ . The same tendency holds for the maximum energy achievable by the electrons. The maximum energy gain without losses coincides with the energy gain one would expect from the potential shown in Fig. 4. Due to the fact, that the minimum energy gain in these distributions is quite constant with respect to a vari-

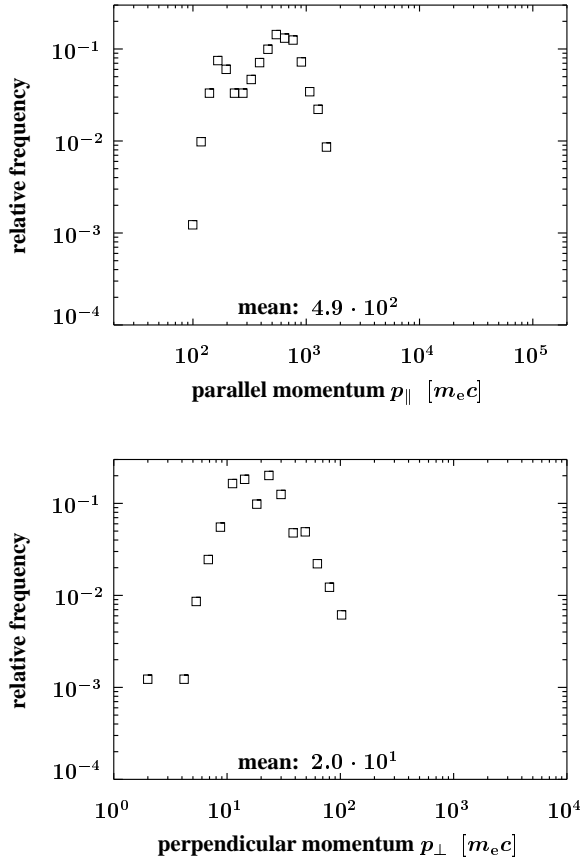


**Fig. 7.** Comparison between the distribution of the final momentum parallel (top) and perpendicular (bottom) to the magnetic fieldlines (Note that the abscissae are different in the two figures)

ation of  $U_{\text{Rad}}$  (this results from the  $\gamma^2$ -dependence of  $\mathbf{F}_{\text{Rad}}$ ), the distribution becomes steeper and narrower with stronger energy losses.

Fig. 7 shows the distributions of the final momenta of the particles perpendicular and parallel to the magnetic field. It is evident, that the motion of the electrons is strongly anisotropic. They are mainly following the magnetic field lines, whereas any motion vertical to the field lines is suppressed. Thus, one may conclude that the accelerated electrons represent a collection of quasi-monoenergetic beams. It is not shown, that the movement becomes the more isotropic, the higher the losses are. But this is straightforward, because in the loss force used  $\mathbf{F}_{\text{Rad}}$  we have assumed an isotropic photon bath which naturally tends to isotropize the electron orbits.

In Fig. 6 and Fig. 7 (top) one also can see another characteristic feature of our field configuration. It is quite obvious that in all four distributions there is something like an absorption line between the two local maxima. This effect can be explained in a natural way, if one looks directly at some chosen trajectories of the particles. Fig. 8 shows the trajectories of the electrons in combination with a projection of the orbits on the

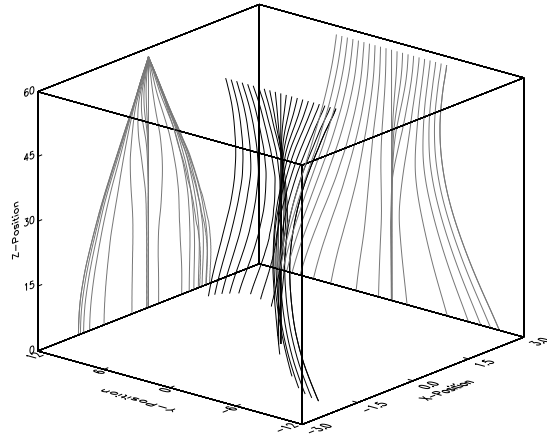


**Fig. 8.** Trajectories of a chosen set of electrons. The projections on the walls behind, were added artificially for a better 3-D impression.

walls behind. These projections show, that there are two populations of electrons. One population is accelerated towards and into the central region of reconnection, whereas the other population is repelled. A comparison of the final energies of the electrons with the membership in one of the two classes shows that exactly these electrons which are forced into the reconnection zone are accelerated the most. The members of the other group of electrons only gain some moderate amount of energy. This indicates that the instability of the orbits is the cause for the appearance of the "absorption line". This effect is quite interesting, because it represents a selection process, which leads to an even stronger beaming of the attracted electrons and to an even stronger anisotropy.

#### 4. Summary and Discussion

We addressed the question of charged particle acceleration during magnetic reconnection processes by means of relativistic test particle simulations. Whereas this point is crucial for a great variety of cosmic plasmas in this contribution we dwelled on the pre-acceleration problem in the AGN context. Possible further applications include among others as different plasma systems as the terrestrial discrete auroral arcs, the solar coronal flares, radio activity in T-Tauri magnetospheres, non-thermal emission at the edges of high-velocity clouds that hit the galactic plane and the generation of electron beams in the magnetospheres of neutron stars. The starting point for our present investigations are results obtained by an MHD simulation study (LB). In contrast to previous work carried out by different other groups, we were able to study particle acceleration in large-scale non-linearly developed reconnection electromagnetic fields rather than being restricted to the prescription of somewhat idealized analytical field solutions. Moreover, since for the considered parameter regime we have to expect an intense radiation field the test particle simulations were performed including the relevant radiative losses. A very important question is whether charged particles can really be accel-

erated in the reconnection region up to the pretty high energy values one might deduce from the fluid treatment. Our findings indicate that, in fact, as expected from the fluid simulations (LB), leptons can be accelerated in reconnection zones located in AGN coronae up to high Lorentz factors; i.e. a significant portion of test particles gain about the maximum energy provided by the generalized field-aligned electric potential structures formed during the magnetic reconnection processes we have modeled within the framework of MHD. Thus, particle acceleration in reconnection zones may be considered as a way out of the injection problem we face in the AGN context.

Since sheared magnetic fields can be expected as a very common phenomena in cosmic environments like accretion disks, stellar coronae and interstellar medium, we think that our relativistic particle studies can be regarded as realistic with respect to the used configuration and the dominant forces. In this contribution the magnetic reconnection process is driven by some resistive mechanism originating from plasma instabilities. The excited electromagnetic oscillations serve as resistance. We note that in plasmas which are collisionless (both no Coulomb collisions and no turbulent wave excitation), the particle inertia presents the ultimate source of resistivity and for the magnetic dissipation. The sheared magnetic fields in collisionless systems evolve into very thin filaments, in which the lifetime of the particle determines the electrical conductivity, thereby allowing for efficient dissipation via effective particle acceleration (Lesch and Birk 1998).

Our simulations are test-particle simulations, thus, we plan for future studies to include, additionally, ponderomotive forces and the back reaction of the current carried by the high energy particles. Whether or not the latter aspect becomes important depends on the density of the run-away electrons limited by the Dreicer electric field (e.g. Benz 1993).

*Acknowledgements.* This work was supported by the the Deutsche Forschungsgemeinschaft through the grant LE 1039/3-1.

## References

- Abraham, Z. et al: 1994, *Compact Extragalactic Radio Sources*, eds. J.A. Zensus & K.I. Kellermann, Proc. NRAO, Socorro, p.87
- Benz, A.O.: 1993, *Plasma Astrophysics*, Kluwer, Dordrecht
- Birk, G.T., Otto, A.: 1996, *J. Atm. Sol.-Terr. Phys.* 59, 835
- Blandford, R.D.: 1994, *ApJS* 90, 515
- Burke, B.F., Graham-Smith, F.: 1997, *Radio Astronomy*, Cambridge University Press, Cambridge
- Camenzind, M.: 1990, in *Reviews in Modern Astronomy* 3
- Cohen, M.H. et al.: 1977 *Nature* 268, 405
- Dermer, C.D., Schlickeiser, R.: 1993, *ApJ* 416, 458
- Done, C., Fabian, A.C.: 1989, *MNRAS* 240, 81
- Galeev, A.A., Rosner, R., Vaiana, G.S.: 1979, *ApJ* 229, 318
- Huba, J.D.: 1985, in *Unstable Current Systems and Plasma Instabilities in Astrophysics*, IAU 107, eds. M.R. Kundu, G.D. Holman, Reidel, Dordrecht, p. 315
- Krall, N.A., Trivelpiece, A.W.: 1973, *Principles of Plasma Physics*, Wiley, New York
- Landau, L.D., Lifshitz, E.M.: 1951, *The Classical Theory of Fields*, Pergamon Press, Addison-Wesley Publ. Comp., Reading Mass. USA
- Lesch, H., Birk, G.T. : 1997, *A&A* 324, 461
- Lesch, H., Birk, G.T.: 1998, *ApJ* (in press May 20 issue)
- Melrose, D.B.: 1994, in *Plasma Astrophysics*, eds. A.O. Benz and T.J.-L. Courvoisier, Springer, Heidelberg, p. 113
- Miyoshi, M., Moran, J., Herrnstein, J. et al.: 1995, *Nat.* 373 127
- Nandra, K., Pounds, A.A.: 1994, *MNRAS*, 268, 405
- Parker, E.N.: 1994, *Spontaneous Current Sheets in Magnetic Fields*, Oxford University Press
- Pearson, T.J. et al.: 1981 *Nature* 290, 365
- Schindler, K., Hesse, M., Birn, J.: 1988, *J. Geophys. Res.* 93, 5547
- Schindler, K., Hesse, M., Birn, J.: 1991, *ApJ* 380, 293
- Stella, L. Rosner, R.: 1984, *ApJ* 277, 312
- Svensson, R.: 1987, *MNRAS* 227, 403
- Ulrich, M.-H.: 1991, in *Structure and Emission Properties of Accretion Disks*, IAU Colloq. 129, eds. C. Bertout, S. Collin-Souffrin, J.P. Lasota and J. Tran Than Van, pp.43-55, Edition Frontieres, Gif sur Yvette Cedex, France